

Hydrodynamic Analysis of Laminar Mixed Convective Flow of Ag-TiO₂-Water Hybrid Nanofluid in a Horizontal Annulus

Badr Ali Bzya Albeshri¹, Nazrul Islam^{1,*}, Ahmad Yahya Bokhary¹, Amjad Ali Pasha²

¹ Department of Mechanical Engineering, King Abdulaziz University, Jeddah-21589, Saudi Arabia

² Aerospace Engineering Department, King Abdulaziz University, Jeddah-21589, Saudi Arabia

ARTICLE INFO

Article history:

Received 15 May 2021

Received in revised form 25 June 2021

Accepted 15 July 2021

Available online 31 July 2021

Keywords:

Annulus pipe; buoyancy effect; entrance region effect; hybrid nanofluid; simultaneously developing flow; numerical simulations; Nusselt number

ABSTRACT

Nanofluids occupy a large place in many fields of technology due its improved heat transfer and pressure drop characteristics. Very recently, a new type of nanofluid, known as hybrid nanofluid, which consists of a mixture of two different nanoparticles suspended in the base fluid has been found to be the most emerging heat transfer fluid. It is well also established that entrance region effect enhances heat transfer rate. The present study deals with numerical investigations of the hydrodynamic behavior of the laminar mixed convective flow of a hybrid nanofluid in the entrance region of a horizontal annulus. A thermal boundary condition of uniform heat flux at the inner wall and an adiabatic outer wall is selected. The SIMPLER numerical algorithm is adopted in the present study. The hybrid nanofluid consists of water as base fluid and Ag-TiO₂ as nanoparticles. The ratio of Ag to TiO₂ is maintained as 1:3. The objective of the current study is mainly to analyze the hydrodynamic behavior hybrid nanofluid in the entrance region. The investigation reveals that the effect of the secondary flow due to the buoyancy forces is more intense in the upper part of the annular cross-section. It increases throughout the cross-section until its intensity reaches a maximum and then it becomes weak far downstream. The development of axial flow and temperature field is strongly influenced by the buoyancy forces.

1. Introduction

The first decade in the research on nanofluids has primarily been devoted to the measurement and modeling of fundamental thermophysical properties such as thermal conductivity, density, viscosity, and heat transfer coefficient [1,2]. Nowadays, researchers are trying to explore the performance of nanofluids in a wide variety of engineering applications. Thus, a lot of experimental work, as well as theoretical models, have been reported by the researchers to improve the thermal properties of nanofluids [3-8]. Regarding the selection of the flow geometry, a concentric annular duct has been chosen in the current study. This duct is used in numerous heat transfer and fluid flow devices. For example, the cooling of the nuclear fuel rods requires the consideration of mixed convection heat transfer. The condensers for seawater distillation, underground electric transmission cable using pressurized gas, cooling of turbine rotors, the chemical vapor deposition processes for

*Corresponding author.

E-mail address: nabdulhafiz@kau.edu.sa (Nazrul Islam)

the fabrication of semiconductor devices, the thermal storage systems, the food processes, and the thermal insulation are additional examples where the results of buoyancy-influenced convection heat transfer in annulus pipe are useful. Investigations [7-12] on mixed convection in horizontal annuli revealed that heat transfer augmentation for simultaneously developing flow is higher than that for fully developed flow [13-18]. It has been observed that further improvement in heat transfer performance can be achieved by using nanofluid [19,20] in place of conventional cooling fluids such as water, oil, and air.

Very recently, a new type of nanofluid, known as hybrid nanofluid, which consists of a mixture of two different nanoparticles suspended in the base fluid has been discovered by the researchers [21-24]. Superior thermal characteristics of hybrid nanofluids have not only been declared it to be the most emerging heat transfer fluid but also the most fascinating one for future studies. One such hybrid nanofluid is Ag-TiO₂/water. High thermal conductivity of Ag is an additional benefit of this hybrid nanofluid.

Review of literature reveals that no study on hydrodynamic analyses of hybrid nanofluid in the entrance region of horizontal annulus is reported so far. However, fluid flow in annulus is of great technological importance as annular duct is widely used many industrial applications. Hence, in the present investigation, hybrid nanofluid has been chosen due to its improved thermal characteristics. The analysis has been carried out with steady laminar combined free and forced convection flow in the entrance region of horizontal concentric cylindrical pipes. The nanofluid considered is a suspension of silver (Ag) and titanium oxide (TiO₂) in water. The thermal boundary condition of constant heat flux at the inner wall of the annulus and a thermally insulated outer wall has been considered in the present study. The code reported by Islam *et al.*, [7] has been modified and used to conduct the present study.

2. Numerical Methodology

The physical model considered in the present study is presented in Figure 1. Constant heat flux has been applied at the inner wall of the, while the outer wall is insulated. For the formulation of the problem, it is assumed that the flow is laminar, steady. The variation of density has been considered only in the body force terms. It is also assumed that the flow is hydrodynamically as well as thermally symmetric across the vertical plane ($\theta = 0^\circ$ and $\theta = 180^\circ$) perpendicular to the axis of the concentric pipes. The radii of outer and inner pipes are chosen as 20 mm and 10 mm, respectively. Hence the outer radius (r_o) to inner radius (r_i) ratio, R , is fixed as 2. A length of 50 times the hydraulic diameter $D_h = [2(r_o - r_i)]$ is considered. The outer cylinder is adiabatic while the inner cylinder is maintained at a constant heat flux.

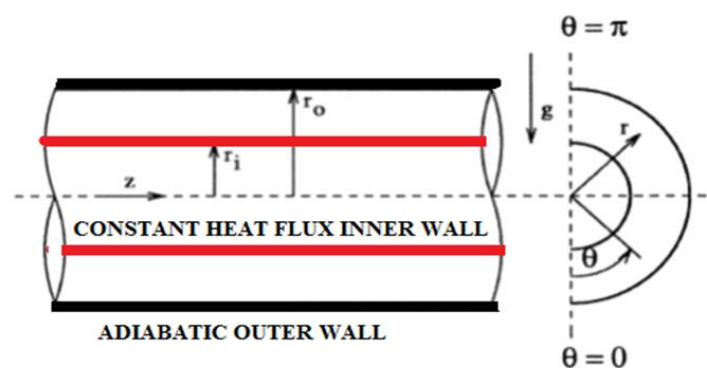


Fig. 1. Schematic diagram of the annulus pipe with boundary conditions

The Boussinesq approximation has been applied in analyzing the problem. All fluid properties other than density are constant. The body force term in the radial momentum equation is

$$g_r = \rho g \cos \theta \quad (1)$$

where ρ is density and g_r is the radial component of acceleration due to gravity, g . Here, θ is measured as shown in Figure 1. The density ρ is given by

$$\rho = \rho_i [1 - \beta(T - T_i)] \quad (2)$$

where ρ_i is the density at inlet temperature T_i and β is the thermal expansion coefficient. The Eq. (1) can be expressed as,

$$\rho g_r = \rho_i [1 - \beta(T - T_i)] \cos \theta \quad (3)$$

The body force term in the θ -direction momentum equation can be similarly written as,

$$\rho g_\theta = -\rho_i g [1 - \beta(T - T_i)] \sin \theta \quad (4)$$

The set of general governing equations are simplified with the above-mentioned assumptions. Continuity equation (conservation of mass)

$$\frac{1}{r} \frac{\partial}{\partial r} (r V_r) + \frac{1}{r} \frac{\partial V_\theta}{\partial \theta} + \frac{\partial V_z}{\partial z} = 0 \quad (5)$$

where V_r , V_θ and V_z are the radial, tangential and axial component of velocity respectively. The conservation of momentum in the radial direction is

$$\frac{1}{r} \frac{\partial}{\partial r} \left[(\rho V_r r) V_r - \mu r \frac{\partial V_r}{\partial r} \right] + \frac{1}{r} \frac{\partial}{\partial \theta} \left[\rho V_\theta V_r - \frac{\mu}{r} \frac{\partial V_r}{\partial \theta} \right] + \frac{\partial}{\partial z} \left[\rho V_z V_r - \mu \frac{\partial V_r}{\partial z} \right] = -\frac{\partial p_c}{\partial r} + \rho g \beta (T - T_i) \cos \theta + \frac{\rho V_\theta^2}{r} - \frac{2\mu}{r^2} \frac{\partial V_\theta}{\partial \theta} - \frac{\mu V_\theta}{r^2} \quad (6)$$

where μ is the dynamic viscosity, T is temperature and p_c is the deviation from the average pressure which is a function of r , θ , and z . The conservation of momentum in the tangential direction is

$$\frac{1}{r} \frac{\partial}{\partial r} \left[(\rho V_r r) V_\theta - \mu r \frac{\partial V_\theta}{\partial r} \right] + \frac{1}{r} \frac{\partial}{\partial \theta} \left[\rho V_\theta V_\theta - \frac{\mu}{r} \frac{\partial V_\theta}{\partial \theta} \right] + \frac{\partial}{\partial z} \left[\rho V_z V_\theta - \mu \frac{\partial V_\theta}{\partial z} \right] = -\frac{1}{r} \frac{\partial p_c}{\partial \theta} + \rho g \beta (T - T_i) \sin \theta + \frac{\rho V_r V_\theta}{r} - \frac{2\mu}{r^2} \frac{\partial V_r}{\partial \theta} - \frac{\mu V_\theta}{r^2} \quad (7)$$

Conservation of momentum in the axial direction

$$\frac{1}{r} \frac{\partial}{\partial r} \left[(\rho V_r r) V_z - \mu r \frac{\partial V_z}{\partial r} \right] + \frac{1}{r} \frac{\partial}{\partial \theta} \left[\rho V_\theta V_z - \frac{\mu}{r} \frac{\partial V_z}{\partial \theta} \right] + \frac{\partial}{\partial z} \left[\rho V_z V_z \right] = -\frac{\partial p}{\partial z} \quad (8)$$

where p is the total pressure.

Conservation of energy

$$\frac{1}{r} \frac{\partial}{\partial r} \left[(\rho V_r) C_p T - r k \frac{\partial T}{\partial r} \right] + \frac{1}{r} \frac{\partial}{\partial \theta} \left[\rho V_\theta C_p T - \frac{k}{r} \frac{\partial T}{\partial \theta} \right] \frac{\partial}{\partial z} [\rho V_z C_p T] = 0 \quad (9)$$

C_p is coefficient of specific heat and k is the thermal conductivity of fluid. The set of governing Eq. (5) to (9) are solved simultaneously for simulating mixed convection phenomenon in horizontal concentric cylindrical pipes. In these equations, the fluid density at the inlet, ρ_i has been denoted by ρ . The boundary conditions in the numerical calculations are

- i. Symmetry lines : ($r_i < r < r_o$; $\theta = 0$ or π) : $V_\theta = 0, \frac{\partial V_r}{\partial \theta} = 0$ and $\frac{\partial T}{\partial \theta} = 0$
- ii. 2) Inner cylinder : ($r = r_i$; $0 < \theta < \pi$) : $V_r = V_\theta = V_z = 0$, and $-k \frac{\partial T}{\partial r} = q$
- iii. 3) Outer cylinder : ($r = r_o$; $0 < \theta < \pi$) : $V_r = V_\theta = 0 = V_z = 0$, and $\frac{\partial T}{\partial r} = 0$
- iv. 4) Inlet: ($z = 0$) : $V_r = V_\theta = 0, V_z = V_{zi}$ and $T = T_i$

The thermophysical properties of ordinary nanofluid are defined as follows

The density of the nanofluid is given by

$$\rho_{nf} = \phi \rho_p + (1 - \phi) \rho_f \quad (10)$$

where ϕ is the volumetric concentration of nanoparticle in nanofluid and the subscripts nf, p and f stand for nanofluid, nanoparticle and base fluid respectively.

Nanofluid heat capacitance

$$(\rho C_p)_{nf} = \phi (\rho C_p)_p + (1 - \phi) (\rho C_p)_f \quad (11)$$

The thermal expansion coefficient of the nanofluid

$$(\rho \beta)_{nf} = \phi (\rho \beta)_p + (1 - \phi) (\rho \beta)_f \quad (12)$$

The viscosity of the nanofluid

$$\mu_{nf} = \frac{\mu_f}{(1 - \phi)^{2.5}} \quad (13)$$

The thermophysical properties of hybrid nanofluid (TiO_2 -Ag- H_2O) are as follows

The density of hybrid nanofluid is specified by

$$\rho_{hnf} = \phi_{TiO_2} \rho_{TiO_2} + \phi_{Ag} \rho_{Ag} + (1 - \phi) \rho_f \quad (14)$$

Here, Φ is considered as the overall volume concentration of two dissimilar types of nanoparticles disseminated in hybrid nanofluid and is considered as

$$\phi = \phi_{TiO_2} + \phi_{Ag} \quad (15)$$

The heat capacitance of hybrid nanofluid is given by

$$(\rho C_p)_{hnf} = \phi_{TiO_2} \rho_{TiO_2} C_{pTiO_2} + \phi_{Ag} \rho_{Ag} C_{pAg} + (1 - \phi)(\rho C_p)_f \quad (16)$$

The thermal conductivity coefficient is determined by

$$\frac{k_{hnf}}{k_f} = \frac{(k_{hp} + 2k_f) - 2\phi(k_f - k_{hp})}{(k_{hp} + 2k_f) + 2\phi(k_f - k_{hp})} \text{ where } k_{hp} = \frac{\phi_{TiO_2} k_{TiO_2} + \phi_{Ag} k_{Ag}}{\phi} \quad (17)$$

The subscript hp stands for hybrid nanoparticles. The governing equations are discretized according to the finite difference method. The present problem has been formulated using a hybrid scheme [25]. After discretization, these equations have been solved simultaneously by following a sequence of steps. SIMPLER [25] algorithm has been adopted in the present work.

The 3-D mesh of the computational domain is shown in Figure 2. A typical finite volume of dimension $\Delta V = r \Delta r \Delta \theta \Delta z$, as shown in Figure 3, is characterized by a node P at the center and six interfaces adjacent to the neighboring nodes in the radial (N and S), angular (W and E) and axial (T and B) directions. All the scalar quantities are stored at the node P, while the vector quantities are crossing through the center of the six faces, n, s, e, w, b and t, surrounding each control volume. The length of the annulus is 1000 mm. To keep the program simple, uniform grids were used in the r- θ coordinates. The effect of grid sizes ($\Delta r \times \Delta \theta \times \Delta z$) on the axial ($Z_n = z/D_h$) variation of Nusselt number is shown in Figure 4. The axial length is denoted by z and Nusselt number, Nu, is defined as

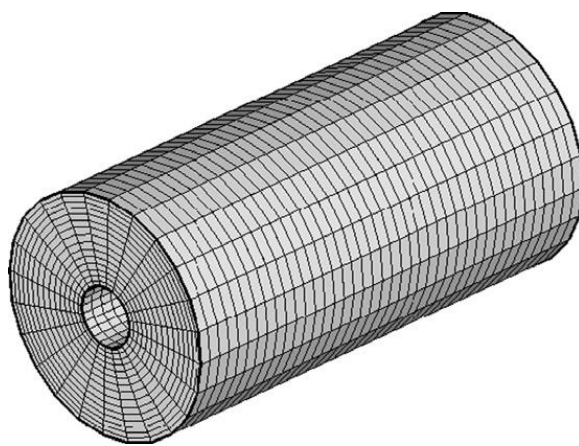


Fig. 2. 3-D mesh of the computational domain

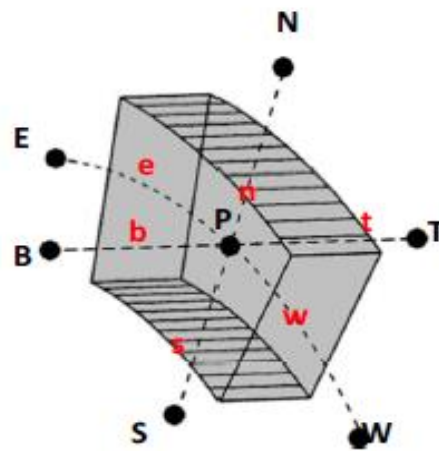


Fig. 3. Typical grid geometry

$$Nu = \frac{h D_h}{k} \quad (18)$$

where h is coefficient of convective heat transfer. To check the grid independence, the results were obtained for radius ratio, $R = 2$, Reynolds number, $Re = 900$, Grashoff number, $Gr = 10^5$ and $\Phi = 0.01$, using five sets of grids: (i) 20x20, (ii) 30x20, (iii) 30x30, (iv) 40x40 and (v) 48x48 grids in the r- θ plane. Re and Gr are defined as,

$$Re = \frac{\rho V D_h}{\mu} \quad (19)$$

$$Gr = \frac{g\beta D_h^4 q}{v^2 k} \quad (20)$$

where v is the kinematic viscosity and q is the wall heat flux. Based on the grid independence test results, a 48x48 grid in the $r-\theta$ plane has been chosen with the number of grids in the axial direction equal to 4000. Hence, for a uniform mesh for an axial length of 1.0 m, $\Delta z=0.25$ mm.

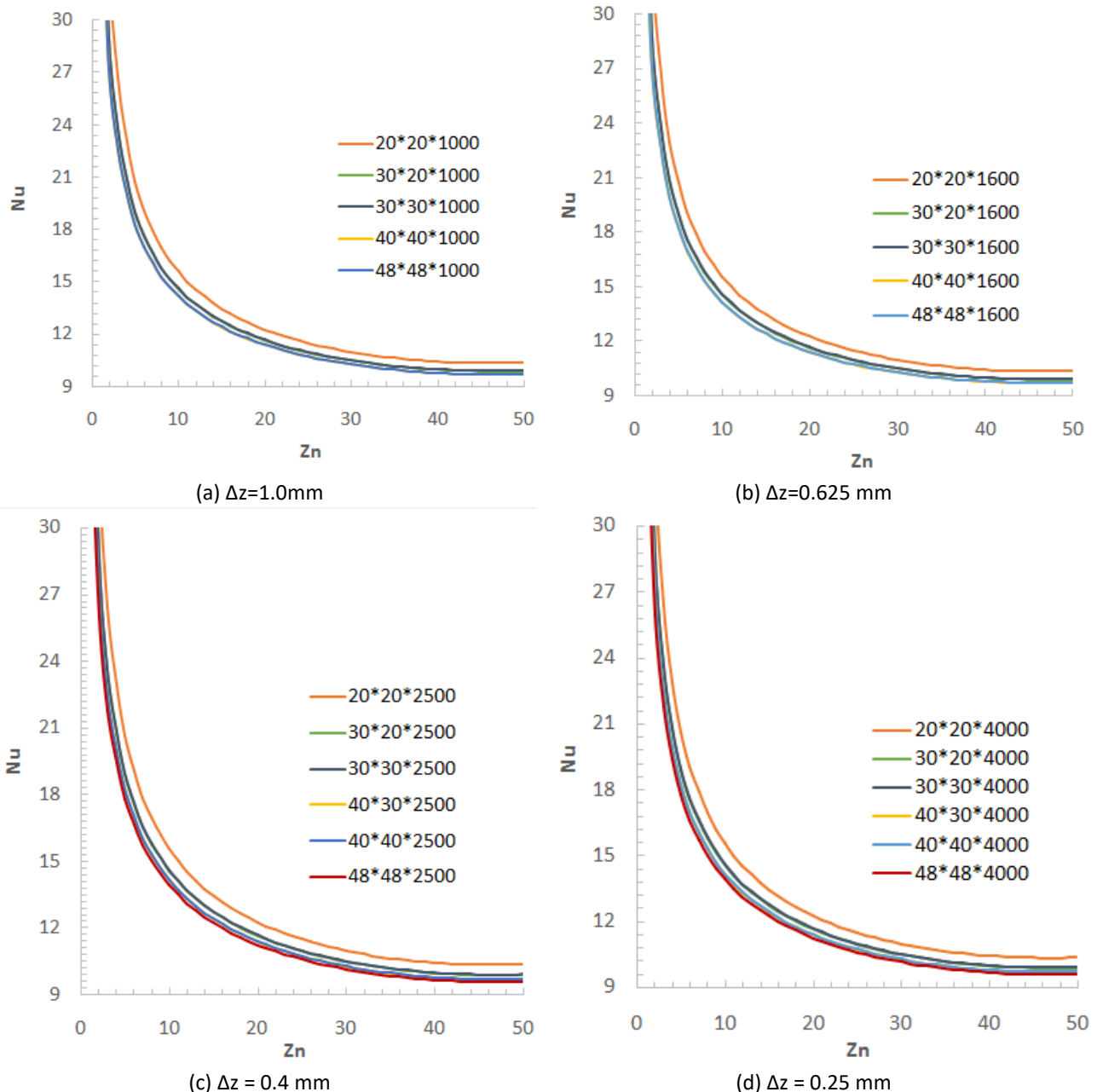


Fig. 4. Effect of different grid sizes in $r-\theta-z$ directions on axial Nusselt number for $Re=900$ and $Gr = 10^5$ and $\Phi = 0.01$

Islam *et al.*, [7] validated their code with the numerical data of Kakac and Yucel [26] for the case of simultaneously developing laminar flow, pure forced convection heat transfer in concentric pipes with constant heat flux at the inner wall and the outer wall being adiabatic. Results of Kakac and Yucel [26] have been consistently checked by Shah and London [27] and Kakac and Yener [28]. The comparison of the radial velocity profiles at different axial locations, starting from the immediate

inlet up to the fully developed situation showed excellent matching. The characteristics of the hydrodynamics of numerical code were further checked by comparing the $Re \times \bar{f}_{app}$ Values with the Shah's [27] correlation. The mean apparent friction factor, \bar{f}_{app} , is defined as

$$\bar{f}_{app} = \frac{\Delta p}{0.5 \rho \bar{V}_z^2} (D_h/z) \quad (21)$$

Here Δp is pressure drop and z is the axial distance. The validity of the code developed by Islam *et al.*, [7] has further been corroborated by the matching experimental data reported by Mohammed *et al.*, [6] and computational works of Moghari *et al.*, [29], Motallebzadeh *et al.*, [30] and Benkhedda *et al.*, [31]. It can be seen from Figure 5 that the results obtained with the present code are in excellent agreement with the results of Moghari *et al.*, [29]. Here, $Z=z/L$, is the dimensionless axial length and L is the length of the annulus.

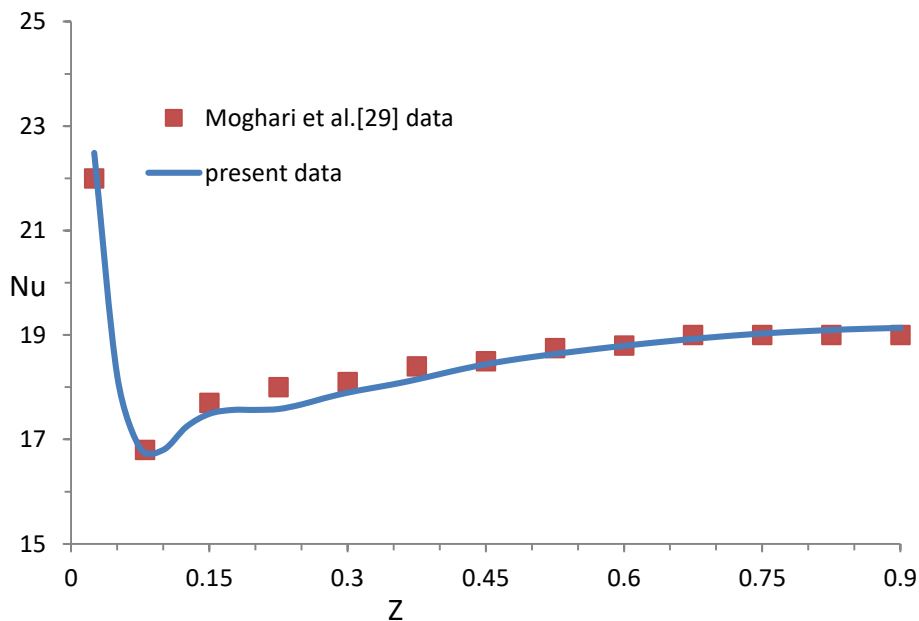


Fig. 5. Verification of the current numerical simulation results with the computed data of Moghari *et al.*, [29]

A mass source, defined as the absolute mass imbalance from the continuity equation is evaluated at each control volume and summed over the entire calculation domain, of 10^{-8} is used to attain the steady-state convergence. The convergence criteria for all the velocities (V_r , V_θ , V_z) is set to an order of less than 10^{-5} and for the fluctuating part of the pressure its of an order of less than 10^{-8} .

3. Results and Discussions

The current numerical investigation has been carried out with $Gr = 10^6$, $R = 2$, $Re = 800$ and $\Phi = 0.04$. The temperature of the nanofluid at the entrance is 25°C . The results are obtained for $0 \leq Z_n \leq 50$, where the velocity ($(V_{rn}=V_r/V_{zi})$, $(V_{thn}=V_{th}/V_{zi})$ and $(V_{zn}=V_z/V_{zi})$) and temperature ($T_n = \frac{(T_f - T_{fi})k}{D_h q}$) profiles are assumed to be almost fully developed. V_{zi} is the axial velocity at the inlet of the annulus and V_{rn} , V_{thn} and V_{zn} are the dimensionless velocities in radial, tangential and axial direction

respectively. T_n is the dimensionless fluid temperature, T_f is the fluid temperature, T_{fi} is the inlet fluid temperature and q is the wall heat flux.

In simultaneously developing flow, as the buoyancy effects become prominent, the isotherms at a cross-section start deviating from the circular shape. The development of isotherms is shown in Figure 6. Near the entrance, at $Z_n = 2.5$ [Figure 6(a)], the isotherms are almost circular and are hardly affected by the secondary flow. Most of the fluid at this location is still at the inlet temperature and the isotherms are almost uniform. As the fluid moves from the inlet of the annulus, the buoyancy forces become significant and start affecting the isotherms. At $Z_n=12.5$ [Figure 6(c)], it is seen that the isotherms at the bottom part ($\theta < 90^\circ$) of the cross-section are still nearly circular and hence, a weak secondary motion in this region. Due to the stronger buoyancy effect in the upper half ($\theta > 90^\circ$) of the cross-section, a noticeable distortion in isotherms is seen in that region. The isotherms at this location tend to become horizontal, approximating the temperature distribution to a stable stratified field. Further downstream, at $Z_n = 50$ [Figure 6(e)], more thermal stratification takes place, and consequently, the buoyancy forces become stable.

The effect of flow development on the radial component of velocity is shown in Figure 7. Near the entrance, at $Z_n=2.5$ (Figure 7(a)), the distortion in the radial isovels is seen to be small and hence, the effect of buoyancy induced flow is not significant in this region. As the fluid moves from the entrance, the buoyancy forces become stronger and start affecting the radial velocity. At $Z_n = 6.25$ (Figure 7(b)), two distinct zones of flow are noticed. In the upper zone of the annulus, radial velocity is positive while in the lower zone the radial velocities are negative. The occurrence of positive radial velocity in the upper part of the annulus may be attributed to the stronger buoyancy effect in that region as clear from the corresponding isotherms in Figure 6. At $Z_n = 12.5$ (Figure 7(c)), a location more away from the inlet, the positive velocity zone is seen to be shifted towards the upper part of the annulus. Also, the emergence of a secondary velocity loop is observed. As the flow develops, further downstream at $Z_n = 50$ (Figure 7(e)), positive radial velocities are seen to be mostly concentrated in the upper part of the annulus owing to the stability of the flow.

The effect of flow development on the tangential component of velocity is shown in Figure 8. Since a flat velocity profile is assumed at the entrance, the angular velocity must be zero at this location. However, because of free convection, even near the entrance, at $Z_n = 2.5$ as shown in Figure 8(a), the emergence of angular velocities is observed. It is seen that the angular velocities are positive near the inner wall and negative near the outer wall. It is also noticed that near the entrance the magnitudes of the angular velocities are small. However, as the flow develops ($Z_n \geq 6.25$), due to stronger buoyancy effects, as clear from the corresponding isotherms in Figure 6, the magnitude of the angular velocities is seen to be increasing.

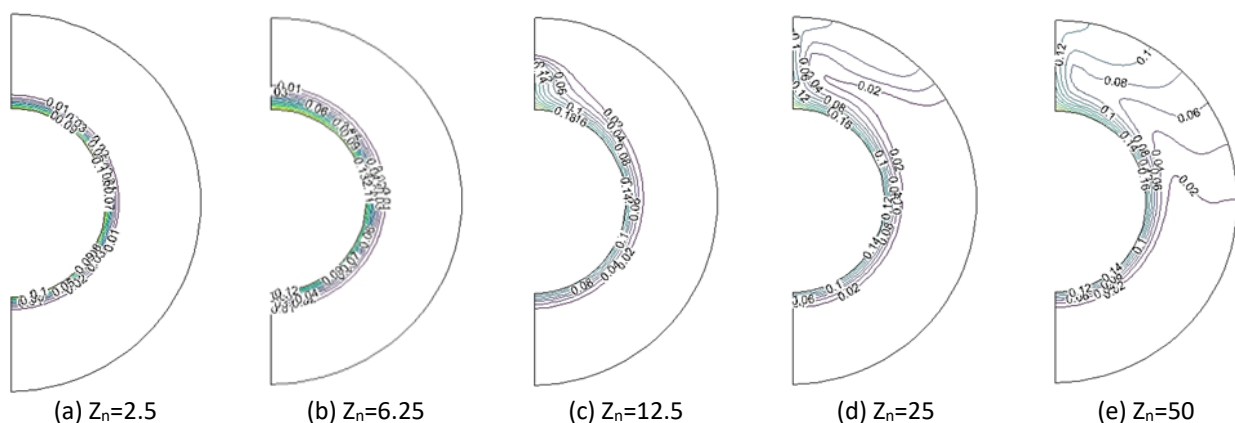


Fig. 6. Development of the isotherm

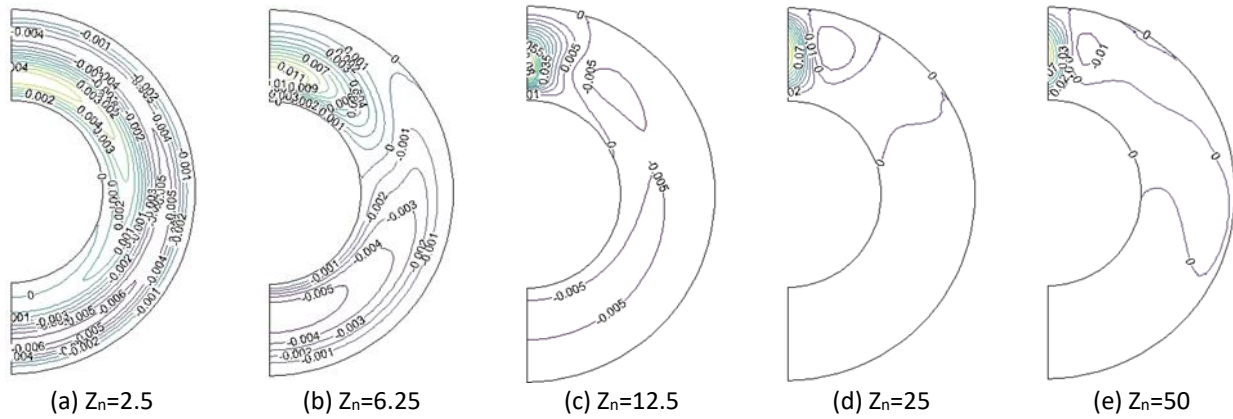


Fig. 7. Development of the radial velocity

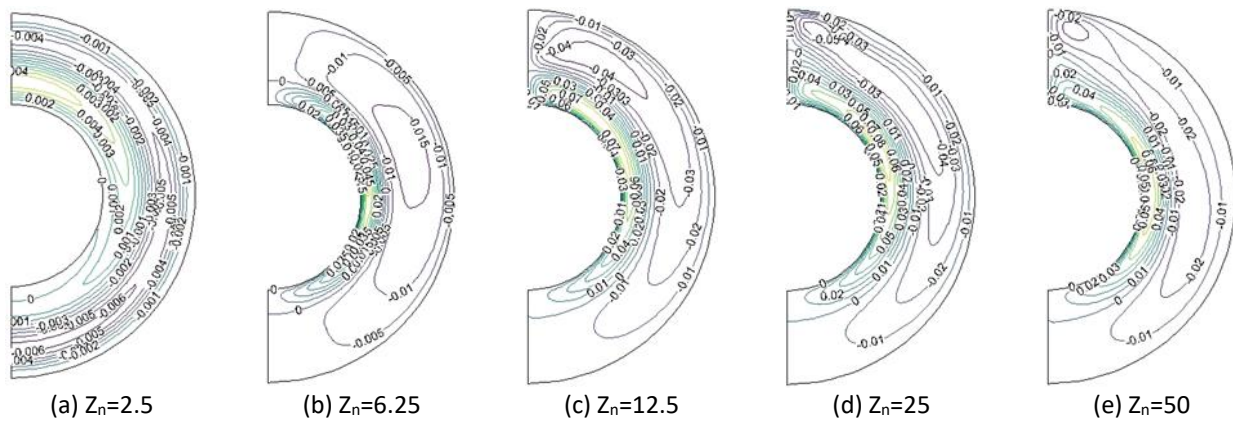


Fig. 8. Development of the tangential velocity

Figure 9 presents the development of dimensionless axial isovels (V_{zn}). The buoyancy-induced secondary flow tends to distort the axial velocity profiles. At $Z_n = 2.5$ in Figure 9(a), a location near the entrance, due to weaker buoyancy effects, as depicted from the isotherms of Figure 6. The axial isovels are circular that resembles the axial isovels for pure forced convection. As the fluid moves away from the inlet, the axial isovels start deviating from the corresponding axial isovels for pure forced convection. It is seen in Figure 9(c), at $Z_n = 12.5$, the axial velocities in the upper half of the annulus are highly distorted due to the stronger buoyancy effect in this region. However, little distortion is observed in the lower half of the annulus. This entails to uneven distribution of mass flux, the minimum being at the top and the maximum at the bottom. Further downstream at $Z_n \geq 25$, the isovels tend to attain the fully developed situation.

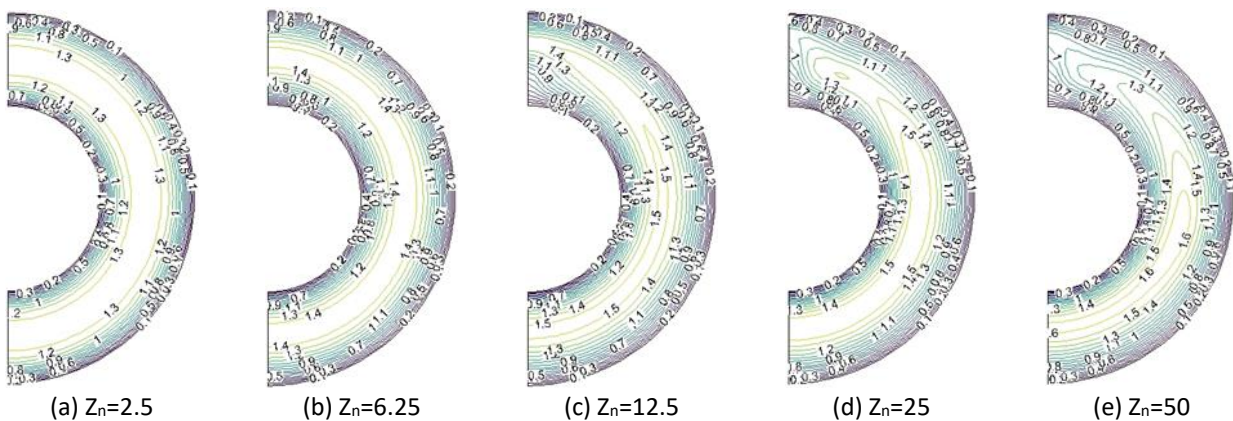


Fig. 9. Development of the axial velocity

Figure 10 presents the effect of the flow development on the variation of radial velocity along the angular direction. As seen in the figure, near the entrance ($Z_n = 2.5$), the radial velocity is almost zero in the lower half ($\theta \leq 90^\circ$) of the annulus and is positive and very small in magnitude in the upper half ($\theta \geq 90^\circ$) of the annulus. At $Z_n = 6.25$, a location slightly away from the entrance, the effect of free convection is still insignificant as clear from the isotherms in Figure 6. As the flow develops ($Z_n \geq 12.5$), the radial velocities are highly affected at the upper half ($\theta \leq 90^\circ$) of the annulus, whereas the radial velocities in the lower half ($\theta \geq 90^\circ$) of the annulus is almost unchanged.

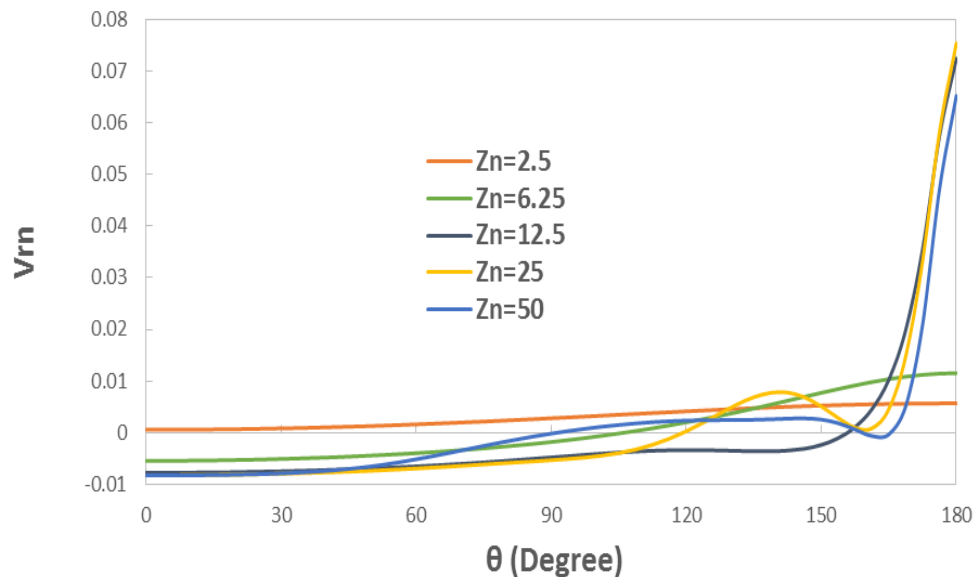


Fig. 10. Effect of flow development on the variation of dimensionless radial velocity (V_{rn}) along the angular direction

Figure 11 shows the effect of flow development on the variation of angular velocity along the radial $r_n = [(r - r_i) / (r_o - r_i)]$ direction. Near the inlet location at $Z_n = 2.5$ of the annuli, the angular velocity near the inner wall ($0 \leq r_n \leq 0.2$) first increases along the radial length and then starts decreasing and finally reverses its direction from positive to negative and remains almost constant in the remaining portion ($0.2 \leq r_n \leq 1.0$) of the annulus. This can well be understood from the isotherms of Figure 6 as the magnitude of isotherms away from the inner wall is very small. As the flow develops ($Z_n \geq 6.25$), the radial velocities are seen to be increasing owing to the effect stronger buoyancy effect. It is observed that with the development of flow, the distribution of the positive velocities is increasing near the inner wall. This distribution is about 40% for the case of $Z_n = 50$.

The effect of flow development in terms of axial velocity profile along the tangential direction is presented in Figure 12. Near the entrance ($Z_n = 2.5$) the axial velocity profile is of semi-flat type indicating inception of flow development. As the flow develops ($Z_n \geq 6.25$) the location of maximum axial velocity shifts towards the inner wall. This may be attributed to the effect of stronger buoyancy forces near the inner wall, which is a constant heat flux, as depicted from Figure 6.

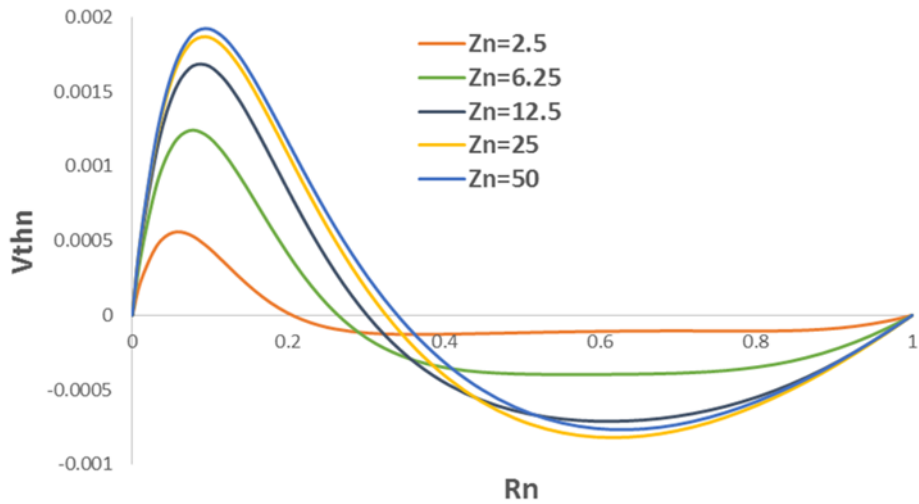


Fig. 11. Effect of flow development on the variation of dimensionless angular velocity (V_{thn}) along the radial direction

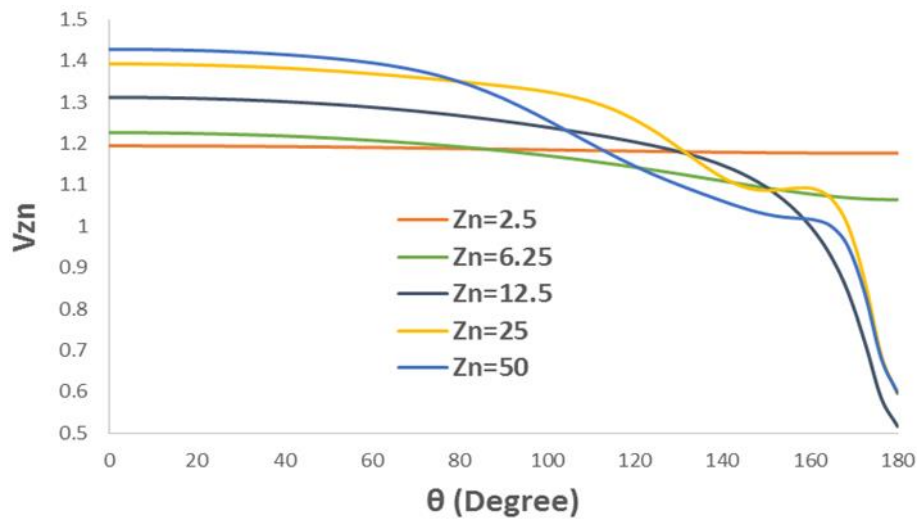


Fig. 12. Effect of flow development on the variation of dimensionless axial velocity (V_{zn}) along the radial direction

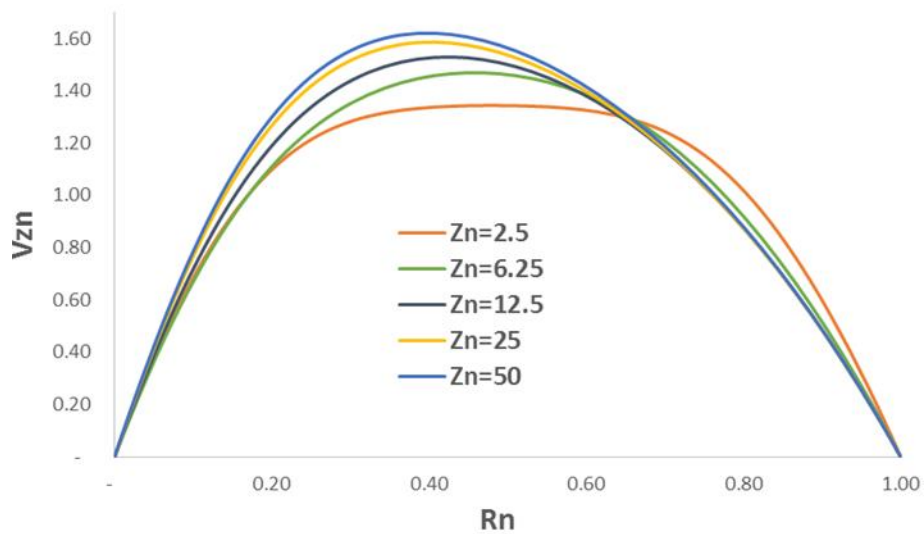


Fig. 13. Effect of flow development on the variation of dimensionless axial velocity (V_{zn}) along the radial direction

4. Conclusions

In the present computational work, investigations have been carried out to study the fluid flow characteristics of a hybrid nanofluid with Ag-TiO₂ nanoparticles dispersed in water for mixed convection situation in the entrance region of the horizontal concentric annulus. The investigation reveals that the effect of secondary flow due to the buoyancy forces is stronger in the upper half of the annular cross-section. It increases throughout the cross-section until its intensity reaches a maximum, and then it becomes weak far downstream. The development of axial flow and temperature field is strongly influenced by the buoyancy induced secondary flow. The buoyancy influence is stronger near the inlet section where it is characterized by a deceleration of the axial flow in the upper part of the annulus and an acceleration of the axial flow in the lower part of the annulus.

Acknowledgement

We would like to thank the high-performance centre staff for providing us the Aziz supercomputing facility to perform the numerical simulations. (<http://hpc.kau.edu.sa>).

References

- [1] Maleki, Akbar, Arman Haghghi, and Ibrahim Mahariq. "Machine learning-based approaches for modeling thermophysical properties of hybrid nanofluids: A comprehensive review." *Journal of Molecular Liquids* (2020): 114843. <https://doi.org/10.1016/j.molliq.2020.114843>
- [2] Sheikholeslami, Mohsen, and Davood Domairry Ganji. *Applications of nanofluid for heat transfer enhancement*. William Andrew, 2017.
- [3] Siddique, M., and A. R. Khaled. "A., Abdulhafiz, NI y A. Boukhary Y.(2010)." *Recent Advances in Heat Transfer Enhancements: A Review Report. International Journal of Chemical Engineering* 1: 1-28. <https://doi.org/10.1155/2010/106461>
- [4] Chandrasekar, M., S. Suresh, and A. Chandra Bose. "Experimental investigations and theoretical determination of thermal conductivity and viscosity of Al₂O₃/water nanofluid." *Experimental Thermal and Fluid Science* 34, no. 2 (2010): 210-216. <https://doi.org/10.1016/j.expthermflusci.2009.10.022>
- [5] Jung, Jung-Yeul, Changhwan Cho, Wook Hyun Lee, and Yong Tae Kang. "Thermal conductivity measurement and characterization of binary nanofluids." *International Journal of Heat and Mass Transfer* 54, no. 9-10 (2011): 1728-1733. <https://doi.org/10.1016/j.ijheatmasstransfer.2011.01.021>
- [6] Saidur, Rahman, K. Y. Leong, and Hussein A. Mohammed. "A review on applications and challenges of nanofluids." *Renewable and sustainable energy reviews* 15, no. 3 (2011): 1646-1668. <https://doi.org/10.1016/j.rser.2010.11.035>
- [7] Islam, Nazrul, U. N. Gaitonde, and G. K. Sharma. "Mixed convection heat transfer in the entrance region of horizontal annuli." *International journal of heat and mass transfer* 44, no. 11 (2001): 2107-2120. [https://doi.org/10.1016/S0017-9310\(00\)00223-4](https://doi.org/10.1016/S0017-9310(00)00223-4)
- [8] Mohammed, Hussein A., Antonio Campo, and Rahman Saidur. "Experimental study of forced and free convective heat transfer in the thermal entry region of horizontal concentric annuli." *International Communications in Heat and Mass Transfer* 37, no. 7 (2010): 739-747. <https://doi.org/10.1016/j.icheatmasstransfer.2010.04.007>
- [9] Halder, S. C. "Combined convection in developing flow through a horizontal concentric annulus." *Numerical Heat Transfer, Part A Applications* 34, no. 6 (1998): 673-685. <https://doi.org/10.1080/10407789808914009>
- [10] Karki, Kailash C., and Suhas V. Patankar. "Laminar mixed convection in the entrance region of a horizontal annulus." *Numerical heat transfer* 15, no. 1 (1989): 87-99. <https://doi.org/10.1080/10407788908944678>
- [11] Terhmina, O., A. Mojtabi, and B. Roux. "A numerical procedure for three-dimensional mixed convection developing flows in an axisymmetric geometry." *European journal of mechanics. B, Fluids* 11, no. 1 (1992): 21-38.
- [12] Nonino, Carlo, and Stefano Del Giudice. "Finite element analysis of laminar mixed convection in the entrance region of horizontal annular ducts." *Numerical Heat Transfer, Part A Applications* 29, no. 3 (1996): 313-330. <https://doi.org/10.1080/10407789608913795>
- [13] Hattori, Naozo, and Susumu Kotake. "Combined free and forced-convection heat-transfer for fully-developed laminar flow in horizontal tubes (experiments)." *Bulletin of JSME* 21, no. 155 (1978): 861-868. <https://doi.org/10.1299/jsme1958.21.861>

- [14] Hattori, Naozo. "Combined free and forced-convection heat-transfer for fully developed laminar flow in horizontal concentric annuli (numerical analysis)." (1979). <https://doi.org/10.1299/kikaib.45.227>
- [15] Nguyen, T. Hung, P. Vasseur, L. Robillard, and B. Chandra Shekar. "Combined free and forced convection of water between horizontal concentric cylinders." (1983): 498-504. <https://doi.org/10.1115/1.3245613>
- [16] Niecekele, A. O., and S. V. Patankar. "Laminar mixed convection in a concentric annulus with horizontal axis." (1985): 902-909. <https://doi.org/10.1115/1.3247519>
- [17] Kaviany, M. "Laminar combined convection in a horizontal annulus subject to constant heat flux inner wall and adiabatic outer wall." (1986): 392-397. <https://doi.org/10.1115/1.3246935>
- [18] Habib, M. A., and A. A. A. Negm. "Laminar mixed convection in horizontal concentric annuli with non-uniform circumferential heating." *Heat and Mass Transfer* 37, no. 4 (2001): 427-435. <https://doi.org/10.1007/s002310000153>
- [19] Das, Sarit K., Stephen U. Choi, Wenhua Yu, and T. Pradeep. *Nanofluids: science and technology*. John Wiley & Sons, 2007. <https://doi.org/10.1002/9780470180693>
- [20] Yu, Wenhua, David M. France, Jules L. Routbort, and Stephen US Choi. "Review and comparison of nanofluid thermal conductivity and heat transfer enhancements." *Heat transfer engineering* 29, no. 5 (2008): 432-460. <https://doi.org/10.1080/01457630701850851>
- [21] Benkhedda, Mohamed, Toufik Boufendi, and S. Touahri. "Laminar mixed convective heat transfer enhancement by using Ag-TiO₂-water hybrid Nanofluid in a heated horizontal annulus." *Heat and Mass Transfer* 54, no. 9 (2018): 2799-2814. <https://doi.org/10.1007/s00231-018-2302-x>
- [22] Japar, Wan Mohd Arif Aziz, Nor Azwadi Che Sidik, Rahman Saidur, Yutaka Asako, and Siti Nurul Akmal Yusof. "A review of passive methods in microchannel heat sink application through advanced geometric structure and nanofluids: Current advancements and challenges." *Nanotechnology Reviews* 9, no. 1 (2020): 1192-1216. <https://doi.org/10.1515/ntrev-2020-0094>
- [23] Xian, Hong Wei, Nor Azwadi Che Sidik, Siti Rahmah Aid, Tan Lit Ken, and Yutaka Asako. "Review on preparation techniques, properties and performance of hybrid nanofluid in recent engineering applications." *Journal of Advanced Research in Fluid Mechanics and Thermal Sciences* 45, no. 1 (2018): 1-13.
- [24] Halim, Nur Fazlin Che, and Nor Azwadi Che Sidik. "Nanorefrigerants: A Review on Thermophysical Properties and Their Heat Transfer Performance." *Journal of Advanced Research in Applied Sciences and Engineering Technology* 20, no. 1 (2020): 42-50. <https://doi.org/10.37934/araset.20.1.4250>
- [25] Patankar, Suhas V. "Numerical Heat Transfer and Fluid Flow," McGraw-Hill, New York." (1980).
- [26] Kakac S. and Yucel O. "Laminar flow heat transfer in annulus with simultaneous development of velocity and temperature fields." *Technical and Scincntifec Council of Turki, TUBITAK, ISITEK*, no.19 (1974).
- [27] Shah, Ramesh K., and Alexander Louis London. *Laminar flow forced convection in ducts: a source book for compact heat exchanger analytical data*. Academic press, 2014.
- [28] Kakac, Sadik, Yaman Yener, and Anchasa Pramuanjaroenkij. *Convective heat transfer*. Vol. 2. Boca Raton, FL: CRC press, 1995.
- [29] Moghari, R. Mokhtari, A. Akbarinia, M. Shariat, F. Talebi, and R. Laur. "Two phase mixed convection Al₂O₃-water nanofluid flow in an annulus." *International Journal of Multiphase Flow* 37, no. 6 (2011): 585-595. <https://doi.org/10.1016/j.ijmultiphaseflow.2011.03.008>
- [30] Motallebzadeh, Roghayyeh, Shahin Hajizadeh, and Mohammad Reza Ghasemi. "Numerical Study of Laminar Mixed Convection Heat Transfer of a Nanofluid in a Concentric Annular Tube Using Two-Phase Mixture Model." *International Journal of Aerospace and Mechanical Engineering* 8, no. 3 (2014): 568-575.
- [31] Benkhedda, F., T. Boufendi, and S. Touahri. "Prediction of nanofluid forced and mixed convection heat transfer through an annular pipe." *International Journal of Materials, Mechanics and Manufacturing* 5, no. 2 (2017): 87-91. <https://doi.org/10.18178/ijmmm.2017.5.2.296>